Proceeding Paper

A Comparative Theoretical and Spectroscopic Study of Aminomethylbenzoic Acid Derivatives as Potential NLO Candidates [†]

Amani Direm [1],* and Koray Sayın [2]

[1] Laboratory of Structures, Properties and Interatomic Interactions LASPI²A, Department of Matter Sciences, Faculty of Sciences and Technology, Abbes Laghrour University Khenchela, Khenchela 40000, Algeria

[2] Department of Chemistry, Faculty of Science, Cumhuriyet University, 58140 Sivas, Turkey; krysayin@gmail.com

* Correspondence: amani_direm@yahoo.fr; Tel.: +213-772-33-0287

† Presented at the 24th International Electronic Conference on Synthetic Organic Chemistry, 15 November–15 December 2020; Available online: https://ecsoc-24.sciforum.net/.

Abstract: Three aminomethylbenzoic acid derivatives were theoretically studied at M062X/6-311++G(d,p) level in a vacuum, namely 2-ammonio-5-methylcarboxybenzene perchlorate (**1**), 4-(ammoniomethyl) carboxybenzene nitrate (**2**) and 4-(ammoniomethyl)carboxybenze perchlorate (**3**). The compounds' structures were fully optimized and compared with the single-crystal X-ray diffraction results, showing a very close agreement with the experimental structural parameters. Their IR, 1H- and 13C-NMR spectra were calculated and examined in detail. Furthermore, the molecular electrostatic potential (MEP) maps of the studied compounds were investigated and the strength of the non-covalent interactions evaluated. In addition to these results, the NLO properties of the three compounds were predicted.

Keywords: aminomethylbenzoic acid derivatives; M06-2X Studies; optimized structure; FTIR; ¹H-NMR; ¹³C-NMR; MEP; non-covalent interactions; hydrogen bonds; NLO properties

1. Introduction

2-carboxy-4-methylaniline (known as 2-amino-5-methylbenzoic acid) and 4-(aminomethyl)benzoic acid (PAMBA) are biologically active molecules serving as pharmaceutical intermediates [1] and their derivatives are considered as potential agents for anti-cancer chemotherapy and evaluated for their cytotoxic activity [2–4]. Furthermore, PAMBA, described for its antifibrinolytic action [5,6], is known with its derivatives to inhibit the proliferation of endothelial cells [7,8] and are additionally proven to be antiproteolytic [9].

A structural survey associated with 2-carboxy-4-methylanilinium derivatives and their related amino acids in the structural database (CSD, Version 5.39 [10]) returned only two hits, namely: 2-carboxy-4-methylanilinium perchlorate (**1**) (CSD refcode: CURKOR [11]) and 2-carboxy-4-methylanilinium chloride monohydrate (CSD refcode: GAZZAK [12]). Furthermore, the zwitterionic form of 4-(aminomethyl)benzoic acid, viz. 4-(ammoniomethyl)benzoate monohydrate (CSD refcode: PONTAP), was reported once in the literature [13], and the database survey showed two hits of (4-carboxyphenyl)methanaminium salts (the nitrate derivative (**2**), CSD refcode: CURCUX and the perchlorate salt (**3**), CSD refcode: CURLAE) [11].

Quantum chemical calculations have been considered an attractive research area in the last few years [14–17]. Therefore, modelling studies of the salts (1)–(3) were carried out by using the M06-2X with a 6-311++G(d,p) basis set in the gas phase and the struc-

tures of the three compounds were fully optimized at the same level and compared with the experimental single-crystal X-ray diffraction results previously reported [11]. The IR and the NMR spectra of the mentioned compounds were calculated and examined in detail. Furthermore, the molecular electrostatic potential (MEP) maps of the related compounds were investigated. In addition to these results, the interaction strength between the anions and the cations were calculated and discussed in detail. The NLO behavior of the studied compounds was furthermore theoretically evaluated.

2. Materials and Methods

The computational processes are performed by GaussView 5.0.9 [18] and Gaussian 09 AS64L-G09RevD.01 [19] programs. The M06-2X function of the hybrid density functional theory (DFT) has been derived by Zhao et al. in 2008 [20]. It was adopted in the calculations together with the 6-311++G(d,p) basis set. In the IR computations, no imaginary frequency was observed. As for the NMR spectra of the related compounds, they were calculated with a gauge-independent atomic orbital (GIAO) method. In the calculation of chemical shift values, tetramethylsilane (TMS) was used as a reference substance. Additionally, in the calculations of the MEP maps, the electrostatic potential (ESP) charges were taken into consideration.

3. Results and Discussion

3.1. Comparative Theoretical and Experimental Structural Study

The optimized structures of compounds (**1**)–(**3**) are represented in Figure 1. Selected experimental and calculated geometric parameters are given in Table 1. The accuracy of the calculated results towards the experimental ones was investigated by plotting the scatter graphs. Hence, the regression coefficients (R^2) were calculated from these graphs for each compound and given in the related table.
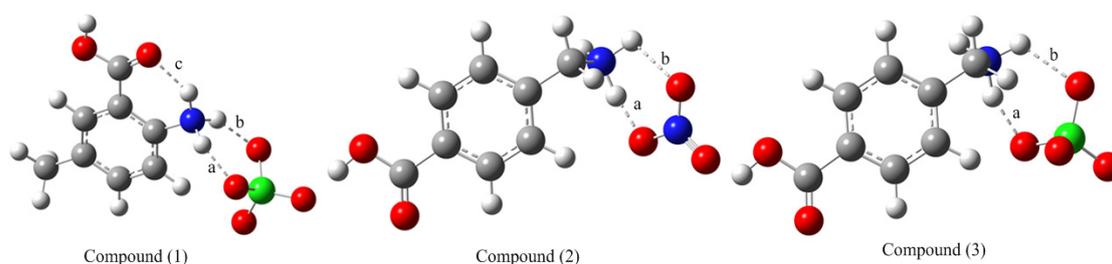

Figure 1. Optimized structures of the studied compounds at the M06-2X/6-311++G(d,p) level in the gas phase.

Table 1. Selected experimental and calculated structural parameters of compounds (**1**)–(**3**).

	Bond Lengths (Å)			Bond Angles (°)	
	Experimental	Calculated		Experimental	Calculated
Compound (**1**) ($R^2 = 0.9998$)					
O1-C7	1.316	1.333	O1-C7-O2	122.5	121.6
O2-C7	1.203	1.212	O1-C7-C1	113.7	113.4
N1-C2	1.465	1.459	O2-C7-C1	123.8	124.9
C1-C2	1.396	1.398	C2-C1-C6	118.7	118.7
C1-C7	1.499	1.486	C2-C1-C7	120.8	121.2
C5-C8	1.507	1.505	C1-C2-N1	121.8	121.3
Compound (**2**) ($R^2 = 0.9998$)					
O1-C7	1.311	1.346	O1-C7-O2	123.3	122.6
O2-C7	1.213	1.200	O1-C7-C1	113.9	112.7
N1-C8	1.486	1.494	O2-C7-C1	122.9	124.6
C1-C2	1.386	1.392	C2-C1-C6	119.4	120.4

C1-C7	1.485	1.491	C2-C1-C7	121.2	121.7
C4-C8	1.505	1.507	C4-C8-N1	112.1	110.2
Compound (**3**) (R^2 = 0.9993)					
O1A-C7A	1.302	1.346	O1A-C7A-O2A	123.7	122.7
O2A-C7A	1.241	1.200	O1A-C7A-C1A	115.3	112.7
N1A-C8A	1.499	1.503	O2A-C7A-C1A	120.9	124.6
C1A-C2A	1.388	1.393	C2A-C1A-C6A	119.8	120.5
C1A-C7A	1.494	1.492	C2A-C1A-C7A	119.3	121.6
C4A-C8A	1.516	1.504	C4A-C8A-N1A	110.6	109.5

According to Table 1, the experimental bond distances vary from 1.203 to 1.507 ♦ for compound (**1**), from 1.213 to 1.505 ♦ for compound (**2**), and in the range 1.241–1.516 ♦ for compound (**3**). These distances are related to the C─CO₂H and C─CH₃/C─CH₂─ bonds. Whereas, the associated calculated values are found to be (1.212–1.505 ♦), (1.200–1.507 ♦) and (1.241–1.516 ♦), respectively. Consequently, the calculated and experimental geometric parameters (bond lengths and angles) are very close to each other and it can be easily seen that there is a good agreement in terms of regression coefficients, with R^2 worth 0.9998, 0.9998 and 0.9993 for compounds (**1**)–(**3**), respectively.

The cationic and anionic moieties in compounds (**1**)–(**3**) were optimized separately at the same level of theory as follow: 2-ammonio-5-methylcarboxybenzene (+1) (**A**), 4-(ammoniomethyl) carboxybenzene (+1) (**B**), perchlorate (-1) (**C**) and nitrate (-1) (**D**) and the total energy of the whole structures are given in Table 2.

Table 2. Total energy of the related structures at the M062X/6-311++G(d,p) level in vacuum.

Moiety	Total Energy (a.u.)	Compound	Total Energy (a.u.)
(**A**)	−515.608	Compound (**1**)	−1276.528
(**B**)	−515.593	Compound (**2**)	−796.100
(**C**)	−760.764	Compound (**3**)	−1276.522
(**D**)	−280.326		

There is an intramolecular hydrogen bond (labeled "c" in Figure 1) in the cationic moiety (**A**) and it is therefore more stable than the cation (**B**). Additionally, there are two other intermolecular hydrogen bonds as labeled in Figure 1 as "a" and "b" in compound (**1**). As for compounds (**2**) and (**3**), they exhibit two intermolecular non-covalent interactions ("a" and "b"). The corresponding interaction energies are calculated as −407.916, −477.384 and −434.142 kJ mol⁻¹ for compounds (**1**)–(**3**), respectively. These results show that the interaction in compound (**2**) is stronger than those of compounds (**1**) and (**3**). It implies that the associated hydrogen bond is stronger due to the electronegative nitrogen atom. The single-crystal X-ray diffraction results [11] show that compound (**2**) displays six strong and moderate O–H…O, O–H…N and N–H…O hydrogen bonds. Whereas in (**3**), it was observed three N–H…O hydrogen bonds only against six O–H…O and N–H…O intermolecular interactions in (**1**).

3.2. Spectral Analyses

The IR spectrum of the studied compounds are calculated and represented in Figure 2a. The most significant bands are labeled in the same figure and the vibration mode and corresponding frequencies are given in Table 3. In Figure 2b, we illustrated the reported experimental FTIR spectra [11].
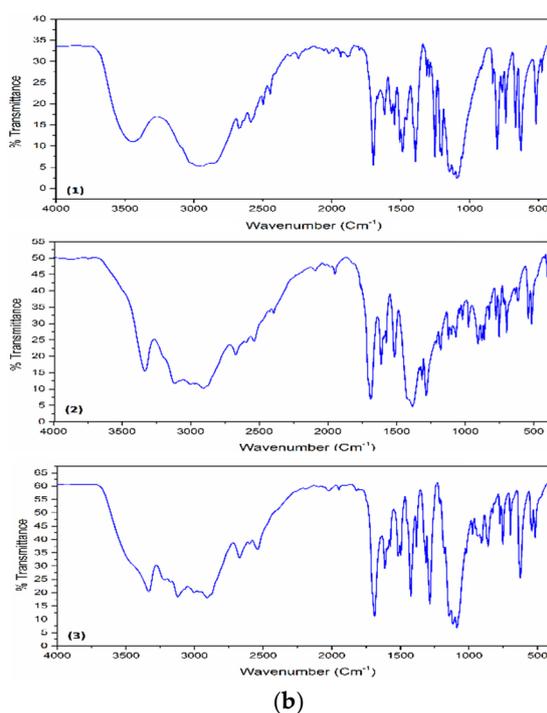
Figure 2. (**a**) IR spectra of compounds (**1**)–(**3**) at the M062X/6-311++G(d,p) level. (**b**) Experimental FTIR spectra of the corresponding compounds.

Table 3. Calculated and experimental vibration modes and wavenumbers (cm^{-1}) of the labeled bands in the IR spectra of the mentioned compounds.

	Compound (1)			Compound (2)			Compound (3)		
Label	Calculated	Experimental	Mode [a]	Calculated	Experimental	Mode [a]	Calculated	Experimental	Mode [a]
1	3832	3446	νOH	3843	3338	νOH	3841	3337	νOH
2	3212	3030	νNH	3106	3119	νNH	3153	3118	νNH
3	3024		νNH	2696		νNH	2873		νNH
4	1817	1698	νC = O	1868	1688	νC = O	1868	1689	νC = O
5	1620	1507	αNH2	1618	1516 1385	αNH2, νN = O	1677	1514	αNH2
		1115						1115	
6	1150	1255	νCl-O, ωCH, ωNH	1355	1283	ωCH	1148	1290	νCl-O, ωCH, ωNH
		1091						1086	

[a] Vibration Modes, ν: stretching; α: scissoring; ω: wagging.

Furthermore, the ^{1}H- and ^{13}C-NMR spectra of the studied compounds were calculated at the same level of theory. The chemical shift values of the related atom are calculated by using TMS. The chemical shift values of the hydrogen and carbon atoms are given in Table 4.

Table 4. Chemical shift values of hydrogen and carbon atoms of the mentioned compounds at the same level of theory.

Assignments	^{1}H-NMR			Assignments	^{13}C-NMR		
	(1)	(2)	(3)		(1)	(2)	(3)
C1	135.8	151.7	152.8	C2H	-	9.03	9.07
C2	151.5	153.0	153.5	C3H	9.52	8.07	8.10
C3	150.0	149.1	148.3	C4H	8.79	-	-
C4	163.6	160.5	158.7	C5H	-	9.64	9.80
C5	164.3	154.7	157.7	C6H	9.15	9.47	9.50
C6	155.5	157.4	157.3	C8H′	3.04	5.03	5.51

C7	185.6	178.3	179.0	C8H″	2.67	3.67	3.66
C8	24.1	49.4	50.7	C8H‴	2.05	-	-
				N1H′	10.88	16.65	11.90
				N1H″	10.79	7.02	7.30
				N1H‴	10.72	3.19	4.29
				O1H	6.48	6.64	6.34

According to Table 4, the chemical shift values of the aromatic carbon atoms are in the range of 135–186 ppm. As for the aliphatic carbons, the chemical shift value is calculated to be 24.1 ppm for compound (**1**) and nearly 50 ppm for compounds (**2**) and (**3**), since the amine group is connected to this carbon in both compounds. The chemical shift values of hydrogen atoms in the aromatic ring are in the range 8–10 ppm vs. 2–5 ppm for the hydrogen atoms connected to the aliphatic carbon. The chemical shift values of some hydrogens are high due to the presence of the hydrogen-bonding networks and the electronegative atoms. These results show that there are three hydrogen bonds in compound (**1**) and two hydrogen bonds in compound (**2**) and (**3**).

3.3. Molecular Electrostatic Potential (MEP) Maps and Contour Diagrams

The molecular electrostatic potential (MEP) maps are important because they allow investigating the active regions, the reaction mechanisms or the interaction regions. The MEP maps of the studied structures are calculated and represented in Figure 3. There are red, yellow, green and blue regions in the figure, which are determined in terms of the electron density. The electronically rich regions are mainly represented in red or yellow whereas the electronically poor ones are displayed in blue. The blue regions are dominant around the hydrogen atoms in the studied compounds, while the red ones are dominant nearby the oxygen atoms which are linked to the chlorine or the nitrogen atoms. The red regions are appropriate to nucleophilic attacks. Particularly, the environment of the carboxyl group and the benzene ring are in the green and yellow. The electron densities are decreasing from red to blue and therefore, the red and yellow regions are more active than the green and blue ones.
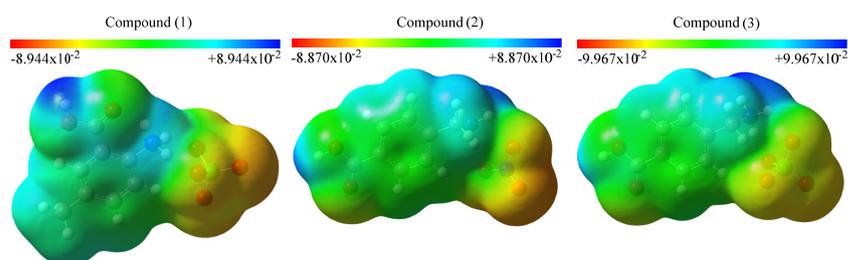

Figure 3. MEP maps of the studied compounds.

The contour diagrams of the frontier molecular orbitals are calculated at the same level of theory and represented in Figure 4.
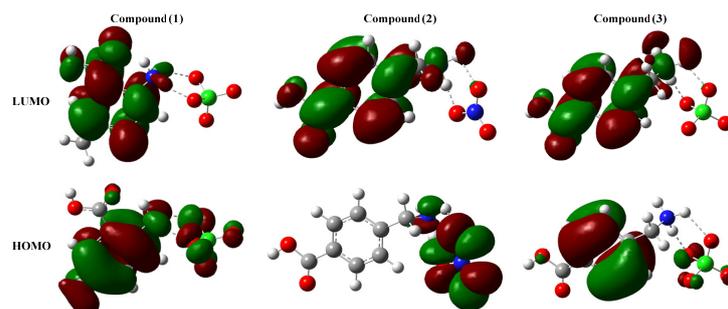

Figure 4. The contour diagram of the studied compounds frontier molecular orbitals.

3.4. Non-Linear Optical Properties

The non-linear optical (NLO) properties can be affected by the molecular structure, the electromagnetic field, the frequency. It is important in providing the key functions of frequency shifting, the optical modulation, the optical switching, the optical logic and the optical memory for the technologies in areas such as telecommunications, signal processing and optical interactions. The NLO properties of the related compounds are predicted by calculating some quantum chemical parameters, which are the total static dipole moment (μ), the average linear polarizability (α), the anisotropy of polarizability ($\Delta\alpha$), and the first hyper polarizability (β). These parameters are calculated by using Equations (1)–(4) and given in Table 5.

$$\mu = (\mu_x^2 + \mu_y^2 + \mu_z^2)^{\frac{1}{2}} \tag{1}$$

$$\alpha = \frac{1}{3}(\alpha_{xx} + \alpha_{yy} + \alpha_{zz}) \tag{2}$$

$$\Delta\alpha = \frac{1}{\sqrt{2}}[(\alpha_{xx} - \alpha_{yy})^2 + (\alpha_{yy} - \alpha_{zz})^2 + (\alpha_{zz} - \alpha_{xx})^2 + 6\alpha_{xz}^2 + 6\alpha_{xy}^2 + 6\alpha_{yz}^2]^{\frac{1}{2}} \tag{3}$$

$$\beta_0 = [(\beta_{xxx} + \beta_{xyy} + \beta_{xzz})^2 + (\beta_{yyy} + \beta_{yzz} + \beta_{yxx})^2 + (\beta_{zzz} + \beta_{zxx} + \beta_{zyy})^2]^{\frac{1}{2}} \tag{4}$$

Table 5. The mentioned quantum chemical parameters for the relevant compounds.

Compound	μ [1]	α [2]	$\Delta\alpha$ [2]	β [3]
Urea	1.76	2.83	10.46	5.09×10^{-28}
(**1**)	4.88	16.48	32.52	1.80×10^{-27}
(**2**)	4.04	15.56	30.68	1.03×10^{-27}
(**3**)	4.40	16.22	33.04	8.88×10^{-28}

[1] in Debye, [2] in $Å^3$, [3] in cm^5/esu.

The NLO properties increase with the increasing of the total static dipole moment, the average linear polarizability, the anisotropy of polarizability and the first hyper polarizability. The related quantum chemical parameters of compounds (**1**)–(**3**) are higher than the urea's values. Therefore, the three compounds are better than urea and could be good candidates for NLO applications. According to the mentioned descriptors and the following ranking:

Compound (**1**) > Compound (**3**) > Compound (**2**) (for μ)
Compound (**1**) > Compound (**3**) > Compound (**2**) (for α)
Compound (**3**) > Compound (**1**) > Compound (**2**) (for $\Delta\alpha$)
Compound (**1**) > Compound (**2**) > Compound (**3**) (for β)

It is worth noted that compound (**1**) is the best candidate for NLO applications.

4. Conclusions

Computational investigations of three aminomethylbenzoic acid derivatives were performed by using the M062X method with the 6-311++G(d,p) basis sets in the gas phase. The structural and spectral analyses were carried out in detail, presenting a very good agreement between the theoretical results and the experimental values. The interaction energies were furthermore calculated and the hydrogen bond strengths of the mentioned compounds were evaluated, showing the presence of intramolecular and intermolecular O–H…O, O–H…N and N–H…O hydrogen bonds. Additionally, the MEP maps of the related compounds were examined and the NLO properties estimated, concluding that the three compounds are good candidates for NLO applications.

References

1. Zheng, B.H.; Fang, Z.J.; Jiao, Y.; Jiang, Y.H. *Jiangsu Chem. Ind.* **2007**, *55*, 39–41, doi:CNKI:ISSN:1002-1116.0.*2007*-01-015.
2. Cao, S.L.; Feng, Y.-P.; Jiang, Y.-Y.; Liu, S.Y.; Ding, G.Y.; Li, R.T. Synthesis and in vitro antitumor activity of 4(3H)-quinazolinone derivatives with dithiocarbamate side chains. *Bioorg. Med. Chem. Lett.* **2005**, *15*, 1915–1917.
3. Cao, S.L.; Feng, Y.P.; Zheng, X.L.; Jiang, Y.Y.; Zhang, M.; Wang, Y.; Xu, M. Synthesis of substituted benzylamino- and hetero-cyclylmethylamino carbodithioate derivatives of 4-(3H)-quinazolinone and their cytotoxic activity. *Arch. Pharm.* **2006**, *339*, 250–254.
4. Cao, S.L.; Guo, Y.W.; Wang, X.B.; Zhang, M.; Feng, Y.P.; Jiang, Y.Y.; Wang, Y.; Gao, Q.; Ren, J. Synthesis and Cytotoxicity Screening of Piperazine-1-carbodithioate Derivatives of 2-Substituted Quinazolin-4(3H)-ones. *Arch. Pharm.* **2009**, *342*, 182–189.
5. Steinmetzer, T.; Pilgram, O.; Wenzel, B.M.; Wiedemeyer, S.J.A. Fibrinolysis Inhibitors: Potential Drugs for the Treatment and Prevention of Bleeding. *J. Med. Chem.* **2020**, *63*, 1445–1472.
6. Markwardt, F.; Neuland, P.; Klöcking, H.P. On the antifibrinolytic activity of the esters of 4-aminomethylbenzoic acid (PAMBA)]. *Pharmazie* **1966**, *21*, 345–348.
7. Pilgrim, H.; Grosse, S. Proliferation of cultured endothelial cells under the effect of aprotinin and 4-aminomethylbenzoic acid. *Biomed. Biochim. Acta* **1986**, *45*, 1015–1019.
8. Kazmirowski, H.G.; Neuland, P.; Landmann, H.; Markwardt, F. Synthesis of antiproteolytic active derivatives of 4-aminomethylbenzoic acid and other structurally similar compounds. *Pharmazie* **1967**, *22*, 465–470.
9. Beyer, S.; Pilgrim, H. The inhibition of endothelial cell proliferation by esters of 4-aminomethylbenzoic acid (pamba). *Pharmazie* **1991**, *46*, 597–599.
10. Groom, C.R.; Bruno, I.J.; Lightfoot, M.P.; Ward, S.C. The Cambridge Structural Database. *Acta Cryst.* **2016**, *B72*, 171–179.
11. Direm, A.; Altomare, A.; Moliterni, A.; Benali-Cherif, N. Intermolecular interactions of proton transfer compounds: Synthesis, crystal structure and Hirshfeld surface analysis. *Acta Cryst.* **2015**, *B71*, 427–436.
12. Dadda, N.; Nassour, A.; Guillot, B.; Benali-Cherif, N.; Jelsch, C. Charge-density analysis and electrostatic properties of 2-carboxy-4-methylanilinium chloride monohydrate obtained using a multipolar and a spherical-charges model. *Acta Cryst.* **2014**, *A68*, 452–463.
13. Atria, A.M.; Garland, M.T.; Baggio, R. Crystal structure of zwitterionic 4-(ammonio-methyl)-benzoate: A simple molecule giving rise to a complex supra-molecular structure. *Acta Cryst.* **2014**, *E70*, 385–388.
14. Sayin, K.; Karakaş, D. Determination of structural, spectral, electronic and biological properties of tosufloxacin boron complexes and investigation of substituent effect. *J. Mol. Struct.* **2017**, *1146*, 191–197.
15. Üngördü, A.; Tezer, N. The solvent (water) and metal effects on HOMO-LUMO gaps of guanine base pair: A computational study. *J. Mol. Graph. Model.* **2017**, *74*, 265–272.
16. Shanmugam, R.; Thamaraichelvan, A.; Viswanathan, B. CO_2 transformation on the active site of carbonic anhydrase enzyme leading to formation of H2CO3-A biomimetic model through computational study. *Turk. Comput. Theor. Chem.* **2017**, *1*, 17–26.
17. Mirzaei, M. 5–Fluorouracil: Computational Studies of Tautomers and NMR Properties. *Turk. Comput. Theor. Chem.* **2017**, *1*, 27–34.
18. Dennington, R., Keith, T., Millam, J. (Eds.) *GaussView*, version 5; Semichem Inc.: Shawnee Mission, KS, USA, 2009.

19. Frisch, M.J.; Trucks, G.W.; Schlegel, H.B.; Scuseria, G.E.; Robb, M.A.; Cheeseman, J.R.; Scalmani, G.; Barone, V.; Mennucci, B.; Petersson, G.A.; et al. (Eds.) *Gaussian 09*, revision A.02; Gaussian, Inc.: Wallingford, CT, USA, 2009.
20. Zhao, Y.; Truhlar, D.G. The M06 suite of density functionals for main group thermochemistry, thermochemical kinetics, non-covalent interactions, excited states, and transition elements: Two new functionals and systematic testing of four M06-class functionals and 12 other functionals. *Theor. Chem. Acc.* **2008**, *120*, 215–241.